Deep drawing simulation of α-titanium alloys using LS-Dyna

Sebastijan Jurendić [a, b], Silvia Gaiani [a, c]

[a] *Akrapovič d.d., Ivančna Gorica, Slovenia*

[b] *University of Ljubljana, Faculty of Mechanical Engineering, Ljubljana, Slovenia*

[c] *University of Modena and Reggio Emilia, Dept. of Materials Engineering, Italy*

Abstract

Titanium alloys have excellent properties for their target applications; however their use is still limited by high price and formability issues. To avoid extensive on-site trials and to cut development costs, a numerical simulation method is developed for the deep drawing process of α-titanium (hexagonal close packed) alloy sheet using LS-Dyna. The Barlat 1989 material model is adopted for modelling the plastic response of the material and the necessary input data is examined. It is found that in order to adequately capture the plastic properties of HCP titanium, load curves are needed both for strain hardening and to capture the strain dependency of the plastic strain ratio. A procedure for determining the material input data from the tensile test results is developed and an exemplary data set is given. To identify a suitable value of the Barlat flow potential exponent m a parametric analysis is carried out using a simulation of the Erichsen cupping test. Forming limit diagrams are adopted for failure prediction, the forming limit curves are determined using the Nakajima method and a simplified procedure for obtaining limiting shear strains on a tensile testing machine is presented. To confirm the method an example of a deep drawn end-cap for a motorcycle exhaust muffler is presented and the simulation compared to the physical forming process with good results.

Keywords: HCP titanium; Forming simulation; Deep drawing simulation; Sheet metal; LS-Dyna;

1 Introduction

With the ever widening field of application of titanium alloys, classical manufacturing techniques are being applied to these high-tech materials. This can pose a problem under mass production conditions, since their relevant mechanical properties are quite different to those of traditional engineering materials.

Such is the case with deep drawing of heat resistant α-titanium alloys for high-end automotive exhaust applications. The exceptional light-weight, mechanical, thermal and corrosion-resistant properties of the finished product outweigh the high cost of the material and complications in the production process. However, difficulties associated with formability of the material need to be overcome in order to establish a reliable production process. This becomes a major issue as the high cost of the raw material, along with relatively low production volumes, makes extensive on-site trials uneconomical. There is a clear need for a numerical simulation method in this field to optimize the process parameters and tooling geometry beforehand and therefore minimize the amount of costly on-site trial and error testing.

A key feature of a method applied in an industrial environment is the ability to promptly and efficiently identify all the necessary input data, especially the material parameters, with readily available tests. The Barlat 1989 material [1] model is well suited in this respect, as it allows for all of its input parameters to be derived from the standard tensile test, which is routinely carried out as part of quality control on incoming raw material.

The aim of this paper is to develop a robust and efficient method for simulating deep drawing of α-titanium alloy sheet using LS-Dyna. The LS-Dyna implementation of the Barlat 1989 material model is reviewed and adopted as the most appropriate material model currently available. The necessary input data for the material model is examined and a material characterization procedure is defined. The Barlat flow potential exponent m is determined through a parametric analysis using a simulation of the Erichsen cupping test.

The α-titanium alloy 1.2 ASN from Kobe Steel is characterized by this method and the data is used on a deep drawing simulation of an exhaust end-cap.

2 General properties of α-titanium and the Barlat 3-paramter material model

2.1 General properties of α-titanium

Titanium alloys used in this application are all based on the α phase with a hexagonal close packed (HCP) crystal structure. A description of the hcp titanium crystal structure and mechanics of deformation is available in [2]. The fundamental properties that make these materials difficult to form and significantly complicate the phenomenological descriptions compared to steels and aluminium alloys are:

- highly anisotropic yielding – high plastic strain ratios that wary greatly with orientation

- highly anisotropic hardening – extension to R_m falls off significantly from longitudinal to transverse direction

- asymmetry in yielding (tensile vs. compressive strength differential – SD) due to twinning phenomena

It should be noted that the twinning deformation mode in titanium is activated during in-plane compression [3].

2.2 Barlat 1989 material model

The Barlat 3-parameter 1989 [1] material model (Material 36 in LS-Dyna) is chosen for the simulations at this stage because it is based on input parameters which have a well defined physical relevance and can be readily measured in an industrial environment on a standard tensile testing machine.

It was developed primarily for BCC and FCC materials and thus lacks the capacity to model SD effects, the yield locus however can be varied trough the flow potential exponent – m to suit the titanium yield surface and should give acceptable results at least under predominantly tensile conditions, where twinning modes are not activated.

According to the Barlat model, the anisotropic plane stress yield criterion is defined as:

$$\Phi = a|K_1 + K_2|^m + a|K_1 - K_2|^m + c|2K_2|^m = 2\sigma_Y^m \quad (1)$$

where K_1 and K_2 are defined as:

$$K_1 = \frac{\sigma_x + h\sigma_y}{2} \quad (2)$$

$$K_2 = \sqrt{\left(\frac{\sigma_x - h\sigma_y}{2}\right)^2 + p^2\tau_{xy}^2} \quad (3)$$

a, c, h, p, m are material parameters defined as:

$$a = 2 - 2\sqrt{\frac{R_{00}}{1 + R_{00}} \cdot \frac{R_{90}}{1 + R_{90}}} \quad (4)$$

$$c = 2 - a \quad (5)$$

$$h = \sqrt{\frac{R_{00}}{1 + R_{00}} \cdot \frac{1 + R_{90}}{R_{90}}} \quad (6)$$

According to the authors of the material model the plastic strain ratio R for an arbitrary angle from the rolling direction can be determined by:

$$R_\phi = \frac{2m\sigma_Y^m}{\left(\frac{\partial\Phi}{\partial\sigma_x} + \frac{\partial\Phi}{\partial\sigma_y}\right)\sigma_\phi} - 1 \quad (7)$$

where the parameter p is calculated iteratively from the above expression to fit the data for the uniaxial tensile test in the diagonal (45°) direction.

The LS-Dyna implementation [4] allows for automatic calculation of the material properties from the plastic strain ratios, which significantly simplifies the use of the model. To account for the anisotropic hardening properties the plastic strain ratio values in the longitudinal, diagonal and transverse direction should be input as functions of equivalent plastic strain, as this will modify the yield locus with the plastic flow.

3 Input parameter determination

3.1 Input parameters

From the mathematical formulation described above, the necessary input data for the constitutive model are:

- Plastic strain ratio in three directions: R_{00}, R_{45}, R_{90}, which are derived directly from the tensile test with the width to thickness strain ratio measurement. To capture the anisotropic hardening the parameters are input as load curves $R_i(\bar{\varepsilon}_P)$.

- Yield stress as a function of equivalent plastic strain $\sigma_Y(\bar{\varepsilon}_P)$ in the rolling direction. Although it is common practice to use the

power law plasticity in forming simulations, this proved inadequate in this application; a full load curve inversely identified from the tensile test should be used instead.

- Flow potential exponent *m* defines the shape of the yield locus. References for this parameter in literature are sparse, however some research on the subject indicates that a quadratic yield locus may be appropriate for titanium [ref], thus *m=2* is used for initial evaluation.

3.2 General mechanical properties of 1.2 ASN

The properties were measured using the standard tensile test in accordance to the EN ISO 6892:2009 standard with the extensometer gauges at 80 mm. The sheet thickness is 0,9 mm. Five samples were tested in each direction, the presented values are average vales of all the tests in their respective directions (*Table 1*).

Table 1
General mechanical properties of 1.2 ASN

Dir.	E [GPa]	R_p [MPa]	R_m [MPa]	A_{gt} [%]	A_{tot} [%]
0°	107	323	457	18,4	32,1
45°	109	355	417	15,7	35,9
90°	109	394	437	9,0	34,5

3.3 Plastic strain ratio

These parameters should be determined first as they are needed in the subsequent steps. They can be determined directly from the tensile test using biaxial strain measurement. The procedure for plastic strain ratio determination is defined in the ISO 10113 standard [5]. This procedure is necessary because of the inherently large error associated with plastic strain ratio measurement [6].

Following the standard procedure, the plastic strain ratios are determined in intervals of 1% from initial yield to the onset of localized necking on the specimen. *Figure 1* shows the variation of the plastic strain ratio with plastic strain. The variation in the longitudinal direction is nearly negligible, in the diagonal and transverse directions there is a significant variation in the initial plastic region before the values stabilize. The curves are extrapolated manually from the onset of necking to large strains using an exponential function. The completed curves are converted into a discreet function to be used as a load curve in the model.
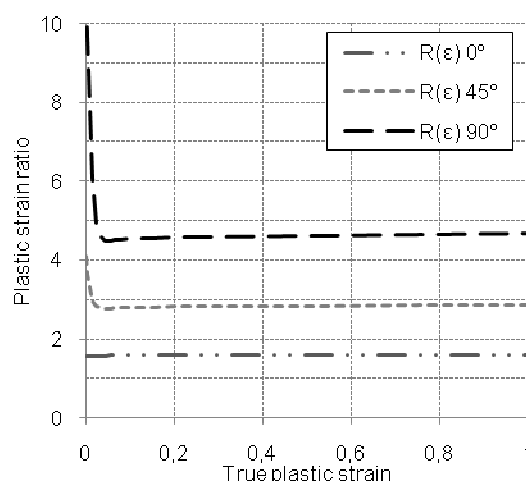

Figure 1. Plastic strain ratio as a function of true plastic strain in the rolling, diagonal and transverse direction.

3.4 Yielding curve determination

Initially the Hollomon equation $\sigma = K \cdot \varepsilon^n$ was used as the yield stress function, however the fit at higher strains is unacceptable. In contrast to steel, titanium exhibits substantial additional elongation past R_m, with a fairly gradual onset of localization, which is in line with the properties expected from its crystal structure.

This phenomenon becomes even more pronounced in the diagonal and transverse directions, where the peak force occurs at very low strains yet the material still achieves a moderate strain at fracture. The assumption follows that quite some useful deformation occurs after the onset of localized thinning in metal forming applications.

This property cannot be reasonably captured by any of the traditional hardening laws, thus a load curve representing yield stress as a function of equivalent plastic strain $\sigma_Y\left(\overline{\varepsilon}_p\right)$ is identified using an inverse procedure proposed by Koc et al. [7].

To summarize, the load curve is identified iteratively by running numerical simulations of the tensile test and comparing the response to the test data. After each iteration the load curve is modified until an acceptable agreement between the simulation and the tensile test is achieved.

A fit within the scatter between samples of the same batch can be achieved without difficulties; however, since the deviation of material properties on a single coil of sheet is usually substantial, a

perfect fit is not necessary. *Figure 2* shows the results of such an inverse procedure, the fit between the measured and calculated σ-ε curves is practically perfect over the entire range of measurement.
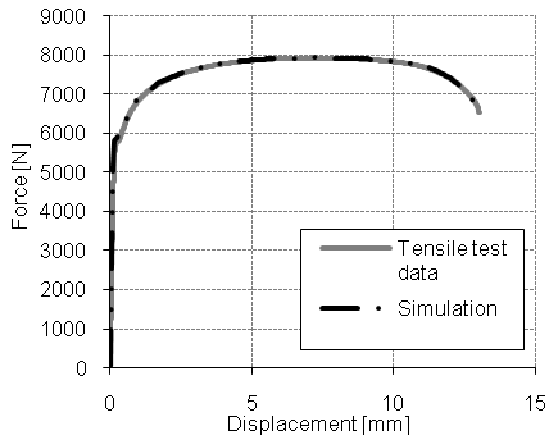

Figure 2. Tensile test simulation vs. the tensile test results.

The final load curve for the material is shown in *Figure 3* along with the measured true stress – true strain curve and the functional approximation using the Hollomon equation. Compared to the Hollomon approximation it is somewhat steeper to support the extensive post-R_m deformation. The load curve is extrapolated past the breaking point, this is necessary as the material can reach much greater stains under different loading conditions, such as biaxial tension.
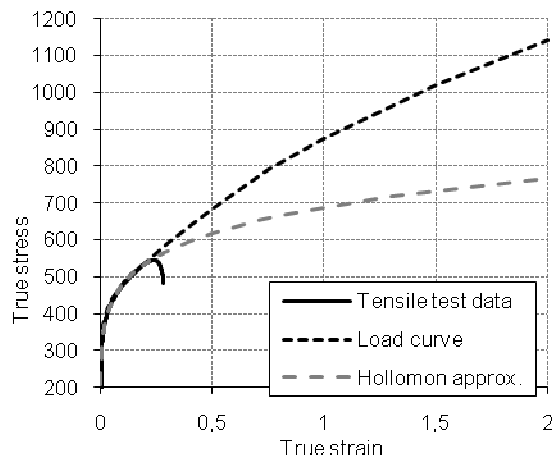
Figure 3. The inversely identified yield curve shown against the Hollomon approximation and the tensile test results.

4 Limits of formability

As the goal of the simulation is to ultimately determine the feasibility of a given deformation process, a way of detecting material defects is needed. For this reason the forming limit diagram (FLD) was determined.

Points on the FLD were measured using the Aramis optical 3D forming analysis system (*Figure 4*) to measure the in-plane strains. This system uses two cameras to recognize a stochastic pattern spray-painted onto the specimens' surface and to track the deformation in real time.
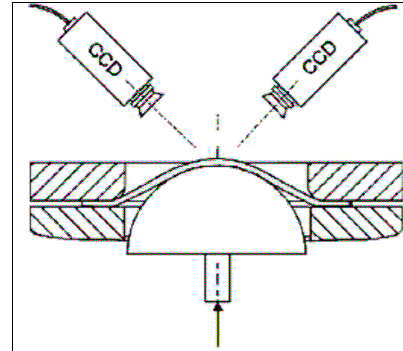

Figure 4. FLD determination with the Aramis system.

In our case the Nakajima method was used to determine the forming limit curve. With this method the minor strain is varied using specimens with different elliptical aspect ratios, as shown in *Figure 5*.
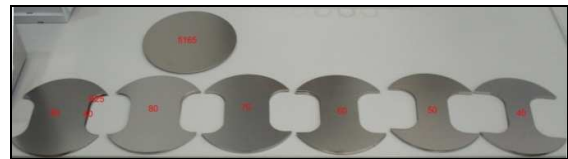

Figure 5. Nakajima test specimens.

The tests have been performed using three specimens for each of the seven different geometries, extracted along the rolling and transverse direction. A total of 42 tests were performed for the material. The forming limit diagrams obtained is shown in *Figure 6*.
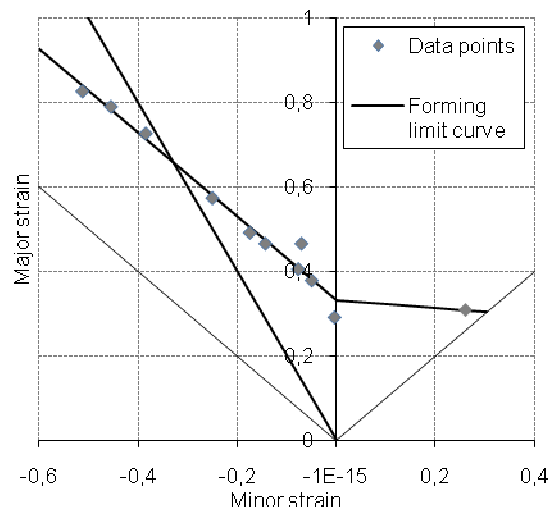

Figure 6. Forming limit diagram for 1.2 ASN.

4.1 Shear forming limit

Failure of the material in shear is a common occurrence in deep drawing processes. If the initial blank size is too small the blank will shear at the die radius. This failure mode is not tested in the conventional Nakajima test, thus a different method has been devised.

A special specimen shown in *Figure 7* has been prepared so that it fits in the standard tensile testing machine to allow for the test to be carried out in-house. The width at the grips is 50 mm and the specimen allows for the use of a standard 80 mm extensometer. The shape was optimized to localize the deformation in the shearing zone.
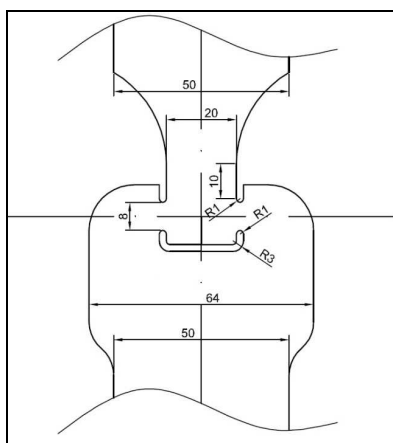
Figure 7. Geometry of the shear test specimen.

The specimen is strained until it breaks and the total extension at the extensometer is noted, a numerical simulation of the test is then carried out to the same amount of deformation.

The numerical model of the specimen is shown in *Figure 8*. It is modelled using three and four node shell elements and symmetry is taken into account.
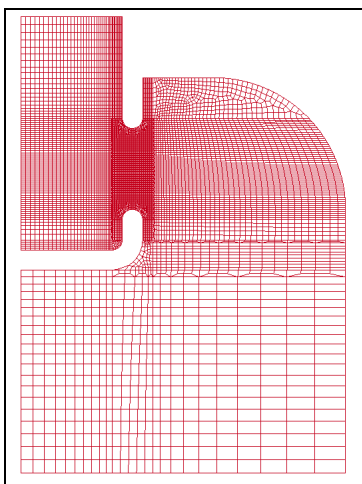

Figure 8. The numerical model for simulating the shear test.

The in-plane strains are plotted in the minor-mayor strain space and a line perpendicular to the upper forming limit line is plotted through the largest negative minor strain as shown in *Figure 9*.
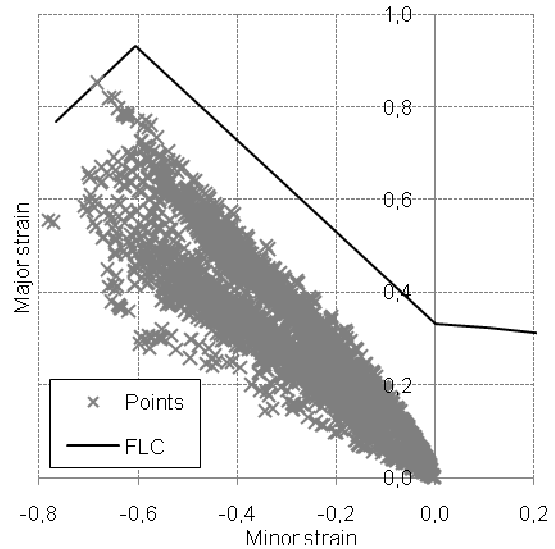

Figure 9. The complete forming limit curve with the in-plane strains from the simulation at specimen fracture.

This is a somewhat simplified approach, however it yields good results as the simulation conditions directly compare to the conditions under which the forming simulations are run.

5 Erichsen cupping test simulation

5.1 The Erichsen test

The Erichsen cupping test is a standard test performed on sheet metal to determine the stretch formability of the material. The test is governed by the ISO 20482 standard. *Figure 10* shows the tooling geometry.
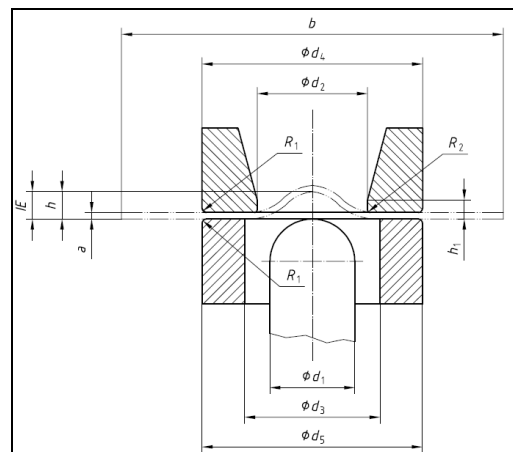

Figure 10. Schematic of the Erichsen cupping test.

This test is particularly well suited for evaluating the material model in the first stage as it strains the specimen in biaxial tension. There is no in-plane compression or shear, thus avoiding the strain differential effects that pose a problem for applications using the Barlat 1989 material model, so it provides a good platform for the parametric analysis of the *m* parameter.

Results of the Erichsen test for the 1.2 ASN material are shown in *Table 2*. The sheet thickness was 0,9 mm and three specimens were tested, the results are average values of all three tests.

Table 2
Erichsen test results for 1.2 ASN

Maximum load [N]	Erichsen index [mm]
22800	8,86

5.2 The numerical model

The numerical model used for the simulations is shown in *Figure 11*, it is comprised of three and four node shell elements. We assume that there is no drawing of the material from under the holder, thus only the free portion on the blank is modelled and fixed around its perimeter in all degrees of freedom, avoiding the need to model the holder. The die and punch are modelled using rigid materials (Material 20 in LS-Dyna) and friction contacts are prescribed between the tools and the blank. The penalty contact formulation proved to be inadequate around the die radius as unacceptable contact penetration occurred and instead a constraint formulation is used. Mass and time scaling are used to cut calculation time, adaptive remeshing was found to not provide a significant time saving in this case, thus a denser mesh was used for the entire simulation.
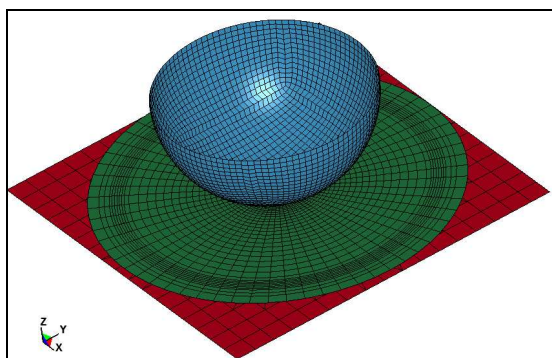

Figure 11. Numerical model of the Erichsen cupping test.

5.3 Parametric analysis results

The results of the parametric analysis, shown in *Figure 12*, indicate that *m=2* is an appropriate value. The force displacement plot shows good agreement between the test and the simulation, also the FLD predicts a break at around 8,7 mm of deflection, which is nearly identical to the test.
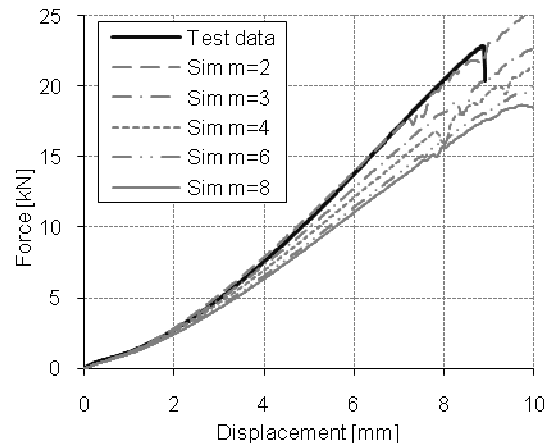

Figure 12. Force – displacement plot of the Erichsen test simulation for different values of *m*.

6 Simulation of a deep drawn part

6.1 The physical part

A motorcycle exhaust end-cap, shown in *Figure 13*, was selected for the simulation. It is a problematic shape to from because of the tapering sides and a small radius at the top. This particular part cannot be drawn from the 1.2 ASN material (the example shown in *Figure 13* is drawn from a different titanium alloy), the material fractures at the leading edge of the punch. This allows for better evaluation of the method as the limits of formability are surpassed.

Figure 13. A fully formed exhaust end-cap.

A series of drawing tests was carried out with the 1.2 ASN material with a sheet thickness of 0,9 mm. Longitudinal and transverse orientations of the material rolling direction with regard to the longer axis of the end-cap were tested and the maximum safe drawing depth for this shape was established to be 47 mm (the full depth is 90 mm). The thickness distribution was then measured on these samples along the line shown in *Figure 14*.

Figure 14. The end-cap drawn to 47 mm with the thickness distribution measurement line.

6.2 The numerical model

Figure 15 shows the numerical model of the end-cap deep drawing process. The model is comprised of three and four node shell elements. As before, the tools are considered rigid and friction contacts are prescribed between the tools and the blank. Even with this larger 5 mm die radius, contact penetration is still an issue for the penalty formulation, and therefore the constraint formulation is used instead. Mass and time scaling as well as adaptive remeshing were used to cut calculation time.
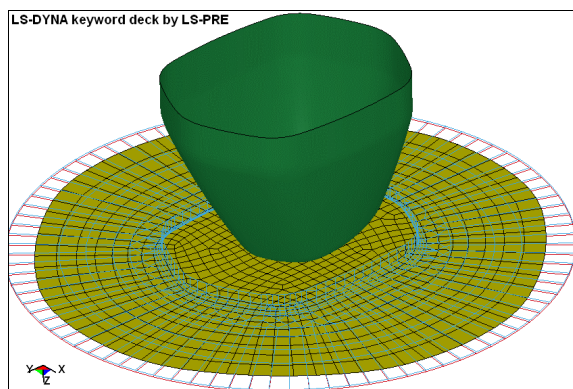

Figure 15. The numerical model of the deep drawing process.

The simulations were run to the full 90 mm drawing depth and both blank orientations were tested.

6.3 Results

The process was evaluated for longitudinal and transverse orientation of the material with regard to the longer axis of the rosette.

The in-plane strains at 47 mm of drawing depth for the longitudinal and transverse directions were plotted on the FLDs in *Figures 16* and *17* respectively. They clearly show the localized deformation in the uniaxial strain region of the FLD that exceeds the forming limit curve. Those points coincide with the leading edge of the punch where fracture occurs.

The simulations predict material fracture on the FLD at around 40 mm of depth for the longitudinal orientations and around 42 mm for the transverse orientation, which is somewhat conservative.
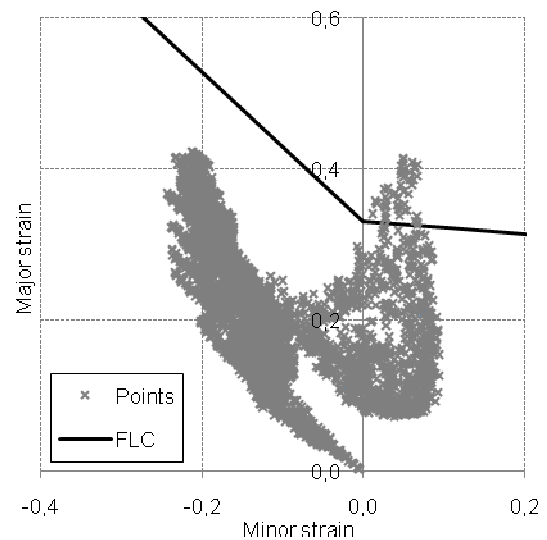

Figure 16. Minor – major strain plot for the longitudinal blank orientation at 47 mm of punch displacement.
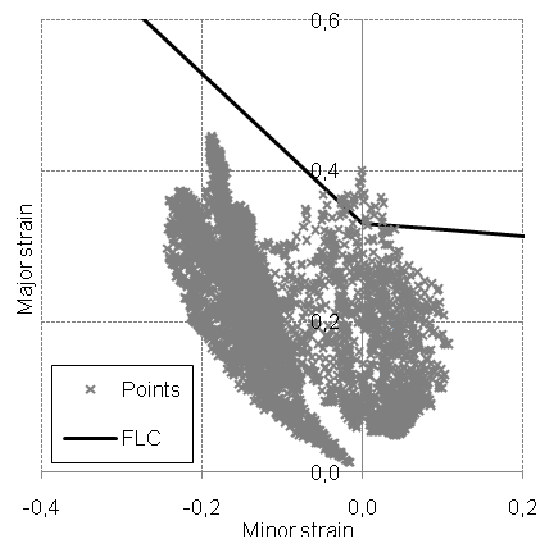

Figure 17. Minor – major strain plot for the transverse blank orientation at 47 mm of punch displacement.

The simulated thickness distributions with both blank orientations at the maximum safe drawing depth were compared to the experimental thickness distributions measured on the real parts. The zero point on the horizontal axis corresponds to the die shoulder, with the distance measured along the surface of the part.

Figures 18 and *19* show the results of the comparison. The simulation results compare fairly well to the measurements; the severe discrepancy in the longitudinal direction is due to the simulation predicting a break in the rosette before this depth is achieved.
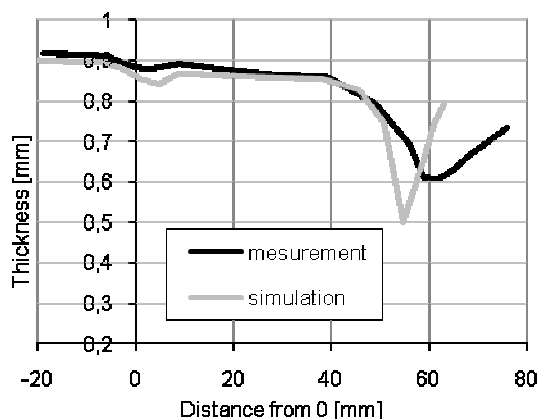

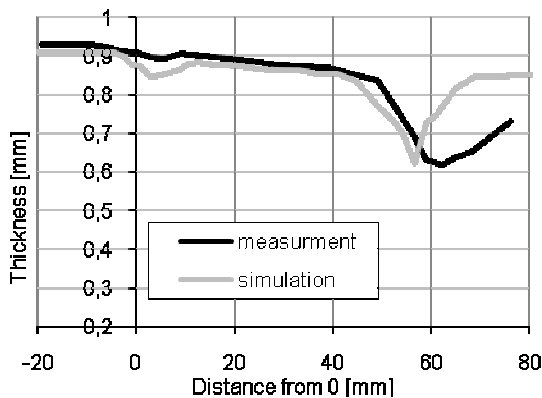Figure 17. Thickness distribution with the longitudinal blank orientation.

Figure 18. Thickness distribution with the transverse blank orientation.

7 Conclusion

Despite the initial concerns about the limitations of the Barlat 1989 material model with regard to HCP materials, the results show that it is quite adequate for simulating deep drawing processes at this level. Both the Erichsen cupping test and the motorcycle exhaust end-cap example show good agreement between the simulation and experiments, although the simulations are somewhat conservative.

The outlined procedure for acquiring material data proved to be quite robust overall. Most of the material data can easily be derived from the tensile test, one area of concern however is the inverse yield curve determination procedure, as it requires manual alterations to the load curve after each iteration, which is unnecessarily time consuming. This process would greatly benefit from automation.

Although the Barlat 1989 model proved to be adequate, there have been recent developments of bespoke HCP material models [8, 9] that could be implemented into LS-Dyna using the UMAT library, and could potentially improve the accuracy of the method, however the determination of the input parameters for these models would require a more complex procedure.

8 References

[1] F. Barlat, J. Lian, Plastic behavior and Stretchability of Sheet Metals, Part 1: A Yield Function for Orthotropic Sheets Under Plane Stress Conditions, International Journal of Plasticity, 5 (1989), p. 51-66.

[2] G. Lutjering, J.C. Williams, Titanium, 2nd edition, Springer, 2007.

[3] M.E. Nixon, O. Cazacu, R.A. Lebensohn, Anisotropic response of high-purity α-titanium: Experimental characterization and constitutive modeling, International Journal of Plasticity, 26 (2010), p. 516-532.

[4] LS-Dyna Keyword Users Manual Volume 2 V971-R4, LSTC, 2009.

[5] International Standard ISO 10113, International Organization for Standardization, 2006.

[6] ASTM Standard E 517-00, ASTM International, 2000.

[7] P. Koc, B. Štok, Usage of the yield curve in numerical simulations, Journal of Mechanical Engineering, 54 (2008), p. 821-829.

[8] O. Cazacu, B. Plunkett, F. Barlat, Orthotropic yield criterion for hexagonal close packed metals, International Journal of Plasticity, 22 (2006), p. 51-66.

[9] M.G. Lee, H.R. Wagoner, J.K. Lee, K. Chung, H.Y. Kim, Constitutive modeling for anisotropic/asymmetric hardening behavior of magnesium alloy sheets, International Journal of Plasticity, 2008 (24), p. 545-582.